catalysts

MDPI

Article

Green Synthesis of Novel *Rhododendron arboreum*-Based Zinc Oxide Nanoparticles for Enhanced Antimicrobial and Photocatalytic Degradation Activities

Sajid Ali [1,*], Sidra [1], Tanveer Asghar [1], Muhammad Ishtiaq Jan [2], Muhammad Waqas [3], Tahir Ali [4], Riaz Ullah [5] and Ahmed Bari [6]

[1] Department of Chemistry, Bacha Khan University, Charsadda 24420, Pakistan; sidraharichand@gmail.com (S.); khantanveer484@gmail.com (T.A.)
[2] Department of Chemistry, Kohat University of Science and Technology, Kohat 26000, Pakistan; mishtiaqjan@kust.edu.pk
[3] Department of Environmental Sciences, Kohat University of Science and Technology, Kohat 26000, Pakistan; waqaskhan@kust.edu.pk
[4] State Key Laboratory of Chemical Oncogenomics, Peking University Shenzhen Graduate School, Shenzhen 518055, China; 2236185106@pku.edu.cn
[5] Department of Pharmacognosy, College of Pharmacy, King Saud University, Riyadh 11451, Saudi Arabia
[6] Department of Pharmaceutical Chemistry, College of Pharmacy, King Saud University, Riyadh 11451, Saudi Arabia; ahmed.bari@gmail.com
* Correspondence: sajidali.faculty@bkuc.edu.pk

Abstract: Zinc oxide nanoparticles (ZnO NPs) are becoming an innovative agent in biological and environmental applications due to its unique characteristics, biocompatibility, low cost and toxicity. In this study, the composite ZnO NPs using *Rhododendron arboreum* (*R. arboreum*) stem bark were synthesized and characterized for UV–visible spectroscopy (UV-vis), Fourier transform infrared spectroscopy (FTIR), energy dispersive X-ray spectroscopy (EDX), scanning electron microscopy (SEM), and X-ray diffraction (XRD). The biomedical assessment of the synthesized nanoparticles showed zones of inhibition of 23 ± 0.09, 18 ± 0.1 and 16 ± 0.05 mm, against the *Klebsiella pneumoniae* (*K. pneumoniae*), *Staphylococcus aureus* (*S. aureus*) and *Escherichia coli* (*E. coli*) strains, respectively. Likewise, the minimum inhibitory concentration (MIC) and minimum bactericidal concentration (MBC) values against *K. pneumoniae*, *S. aureus*, and *E. coli* were found to be 34 ± 0.21 and 72.71 ± 0.47, 47 ± 0.11 and 94.86 ± 0.84 and 94 ± 0.18 and 185.43 ± 0.16 µg/mL, respectively. The biosynthesized ZnO NPs resulted in significant eradication of the outer and inner membranes of the tested bacterial cells. In addition, the environmental application of the synthesized ZnO NPs also showed time-dependent photocatalytic degradation activity and revealed 65% methyl orange dye degradation with an irradiation period of 6 h. The findings of this study suggest the suitability of the novel *R. arboreum* stem bark-based ZnO NPs as an effective ameliorant against bactericidal activities and photocatalytic potential for the removal of potentially toxic substances from water.

Keywords: *Rhododendron arboreum*; zinc oxide nanoparticles; antimicrobial activity; photocatalyst; methyl orange dye

Citation: Ali, S.; Sidra; Asghar, T.; Jan, M.I.; Waqas, M.; Ali, T.; Ullah, R.; Bari, A. Green Synthesis of Novel *Rhododendron arboreum*-Based Zinc Oxide Nanoparticles for Enhanced Antimicrobial and Photocatalytic Degradation Activities. *Catalysts* **2024**, *14*, 337. https://doi.org/10.3390/catal14060337

Academic Editor: Detlef W. Bahnemann

Received: 22 March 2024
Revised: 3 May 2024
Accepted: 7 May 2024
Published: 22 May 2024

1. Introduction

In developing countries, the problem of sanitization, especially waterborne infections, has attained considerable attention over the last few decades [1]. The threats of polluted water may be microbial, chemical, and/or physical [2]. According to Wikipedia, "An infection is the invasion of tissues by pathogens, their multiplication, and the reaction of host tissues to the infectious agent and the toxins they produce". In microbial infections, there is an alarming situation where strong resistance to antibiotics is acquired by a specific microbe(s) [3]. It has been well reported that several groups of antibiotics have become less

effective against several microbial strains. Likewise, among pollutants, dyes are groups of chemicals produced from a series of anthropogenic activities and are released into the water environment [1]. The majority of organic dyes utilized in several industries including those used in textile, paper, paints, and medicine are non-biodegradable [4]. In addition to the environmental problems, dyes are of significant concern because of their extremely hazardous nature causing various health-related problems including excessive perspiration, cognitive confusion, and methemoglobonemia [5]. It has been estimated that during the dyeing process, about 10% of the total dyes are consumed, while all the remaining amount is discharged to the water resources without proper treatment, and hence poses serious threats to the aquatic life by reducing the oxygen supply and the algal photosynthetic ability in water [6].

The researchers are now focused on the development of such strategies to protect human and environmental health effectively and economically [7]. Among the advanced research trends, nanotechnology is an emerging research area in the fields of biomedicine, engineering, and bioremediation [8]. The key features that account for the effectiveness of nanoparticles include small size, high surface area, morphologies, ultraviolet-protective, photocatalytic, and antimicrobial properties that make them a promising candidate in several fields including environment, medicine, and agriculture [9]. Likewise, among nanoparticles, metal-based nanoparticles have gained much attention due to their unique electrochemical, biological and optical properties along with biocompatibility and non-toxic effects [10]. Against microbes, nanoparticles target multiple biomolecules at once and hence prevent the development of microbial resistance [11]. It has been well understood that nanoparticles with antibacterial potentials can reduce the development of resistance in specific microbes [12]. Likewise, due to their unique characteristics including larger excitation binding energy and wide band gap, metal-based nanoparticles are considered an attractive photocatalyst for the degradation of various types of dyes [13].

Nanoparticles can be synthesized through several methods such as microwave, sol-gel, hydrolysis, and co-precipitation methods [14]. However, as compared to other chemical and physical technologies, green nanotechnology is considered an attractive technology due to its low cost and eco-friendly nature. Several researchers successfully investigated the biosynthesis of nanomaterials by using different types of biological sources including bacteria, fungi, and plant extracts [15]. Moreover, the composite of nanoparticles with plants showed better results as compared to other biological systems. In addition, the process of utilizing the plants for green synthesis is economical in comparison to the process involved in using other agents like algae and fungi [16]. Correspondingly, the composite of nanoparticles with various plants and their parts acts differently as both reducing and stabilizing agents [17]. Many plant products have been successfully reported as capping agents for the stabilization of nanoparticles in the literature [18]. However, metal-based nanoparticles using *R. arboreum* stem bark have not received much attention in the literature. *R. arboreum* a member of the family Ericaceae is one of the most important medicinal plants. This plant is distributed throughout the world, but is mostly centered in China, India, Malaysia, and Nepal [19]. In Pakistan, this plant occurs in the Hazara Division and Kashmir. Due to the presence of several bioactive compounds, the various parts of *R. arboreum* have several medicinal applications to treat various diseases including diarrhea, blood dysentery, and headache. The stem bark of the *R. arboreum* contains a variety of compounds which include 15-oxoursolic acid, ursolic acid, betulinic acid, lupeol, taraxerol, β-amyrine, 3-O-acetyl ursolic acid, 3β-acetoxyurs-11-en-13β, 28-olide, 3-O-acetylbetulinic acid [20]. Based on the available information, the current investigation for the first time synthesized ZnO NPs from the bark extract of *R. arboreum* with the aim of exploiting the underlying bactericidal mechanisms against several pathogenic bacteria and its role towards environmental remediation for the photocatalytic degradation of methyl orange dye.

2. Results

2.1. UV–Visible Spectrophotometry and Fourier Transform Infrared Analysis

UV–visible spectrometry is a crucial approach since each metal nanoparticle displayed a different surface plasmon resonance value. The synthesized nanoparticles were therefore validated by UV–visible spectrometry and the results are illustrated in Figure 1a. The spectrum of the surface plasmon resonance at 374 nm suggests the production of ZnO NPs, as seen in the UV–visible spectrum. The biosynthesized ZnO NPs revealed distinctive characteristics of the spectral band that zinc oxide does not exhibit in bulk form. The band gap energy (Eg) of ZnO NPs was determined from UV/Vis absorption spectrophotometry. The Eg was calculated by plotting $(\alpha h\upsilon)^2$ against the photon energy ($h\upsilon$) as shown in Figure 1b. The Eg was calculated from the extrapolation of the linear part of the plot and was found to be 3.2 eV, which was found less than the reported value (3.4 eV) in the literature [21]. Moreover, the FTIR spectra of nanoparticles prepared with *R. arboreum* were also carried out for the determination of various functional groups and the results are shown in Figure 1c. The FTIR spectrum displayed various peaks at 2921, 1700, 1570, 1363, 798, 522, and 453 cm^{-1}. The peaks observed at 2921 and 1700 cm^{-1} correspond to C-H bond stretching and C=O, respectively. Similarly, the peak at 1570 corresponded to the C=C vibration contributed by the aromatic ring while the peak at 1363 indicated the CH_3 bending vibration. The peaks at 798, 522 and 453 cm^{-1} indicated the metal oxide.

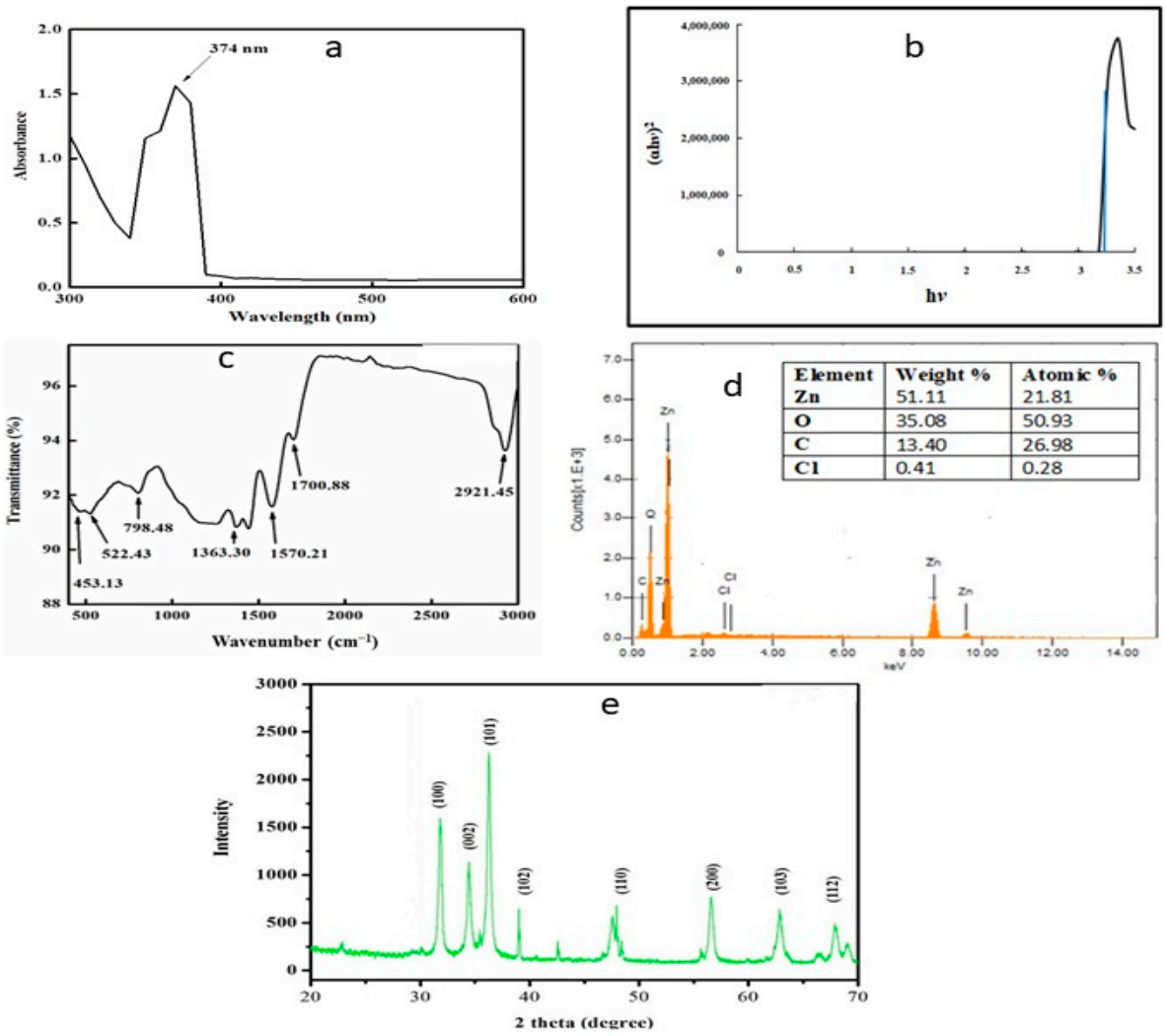

Figure 1. (**a**) UV-Vis absorption spectrum. (**b**) Band gap energy. (**c**) Representative FTIR analysis. (**d**) EDX spectrum. (**e**) XRD analysis of green synthesized ZnO NPs.

2.2. Energy-Dispersive X-ray and X-ray Diffraction Analysis

The EDX analysis showed the presence of various compounds on the surface of the synthesized nanoparticles as shown in Figure 1d. The quantitative and qualitative data from EDX regarding the elemental composition also confirm the synthesis of ZnO NPs. The EDX spectrum of biosynthesized ZnO NPs showed that Zn was present in substantial amounts (51.11%) along with other elements including oxygen (O), carbon (C), chlorine (Cl) that might have derived from the plant extract (Figure 1d). However, the minor peaks for Cl might be also due to the precursor salt used in the synthesis of nanoparticles. Similarly, the XRD analysis of the structure and chemical composition of the synthesized nanoparticles is illustrated in Figure 1e. The results revealed that the sharp diffraction peaks could be used to easily index the hexagonal wurzite structure of ZnO NPs. The peaks (100), (002), (101), (102), (110), (103), (200), and (112) corresponded to 2Θ of 31.821, 34.4651, 36.2886, 47.5941, 56.6508, 62.9114, 66.4064, 67.9868, 69.1113, 72.6063 and 76.9826, respectively. The sample exhibited identical patterns and lacked crystalline impurities, thus indicating the phase purity of ZnO NPs. The crystallite size of the ZnO NPs was also calculated from the intense peak using Scherer's formulae and was found to be 66.20 nm [22].

2.3. Scanning Electron Microscopy and Nano Measurer Particle Size Analysis

The SEM analysis was used to investigate the morphology and microstructure of the synthesized ZnO NPs as illustrated in Figure 2a. The SEM micrograph of the biosynthesized ZnO NPs demonstrated the presence of spherical-shaped nanoparticles. Likewise, the particle size was calculated from SEM images using nano-measurer software, version 1.2.5 (Figure 2b). The results demonstrated that the calculated mean particle size was 9.61 µm.

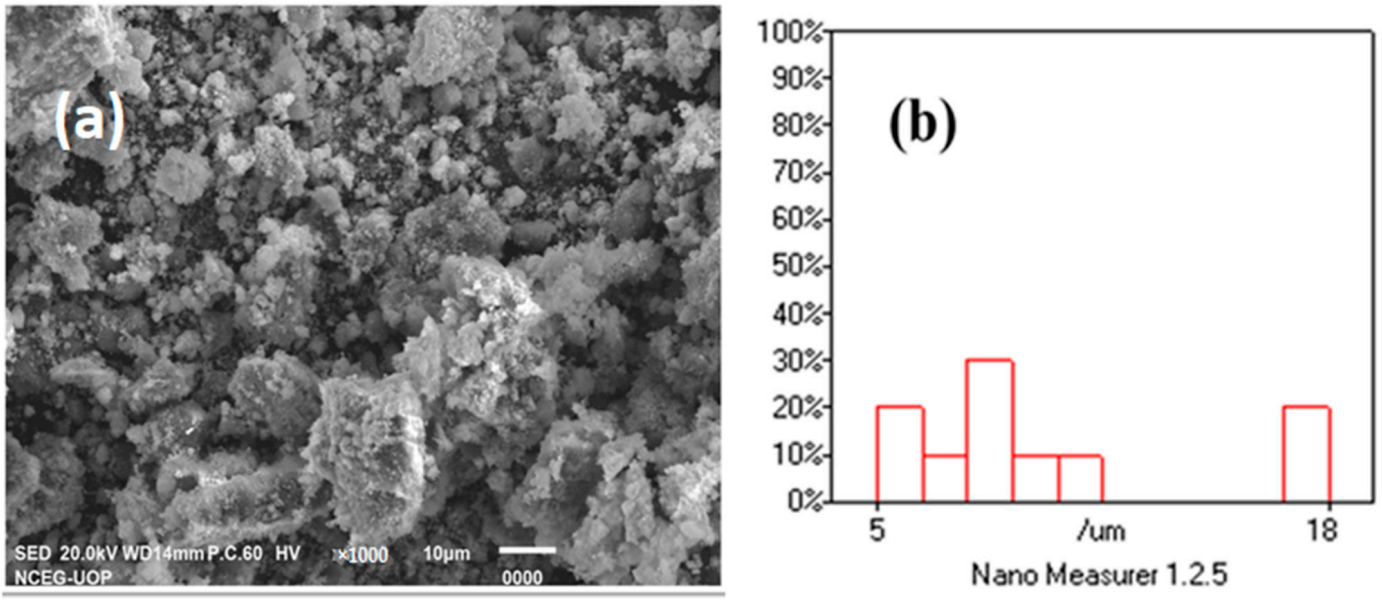

Figure 2. (**a**) Scan electron microscopy image and (**b**) nano-measurer particle size of synthesized ZnO NPs.

2.4. Antibacterial Activity

The findings of the antibacterial potential of the green synthesized ZnO NPs assessed against clinically isolated pathogenic bacteria such as *E. coli*, *S. aureus*, and *K. pneumoniae* are presented in Figure 3. It has been observed that ZnO NPs inhibited the growth of *K. pneumonia* and *S. aureus* with zones of inhibition of 23 and 18 mm, respectively. Likewise in the case of *E. coli* the zone of inhibition was 16 mm. The obtained results are comparable with the tested standard antibiotic levofloxacin as shown in Figure 3. In addition, the investigated MIC and MBC values of the biosynthesized ZnO NPs against *K. pneumoniae*,

S. aureus, and *E. coli* were 34 ± 0.21 and 72.71 ± 0.47, 47 ± 0.11 and 94.86 ± 0.84 and 94 ± 0.18 and 185.43 ± 0.16 µg/mL, respectively (Table 1).

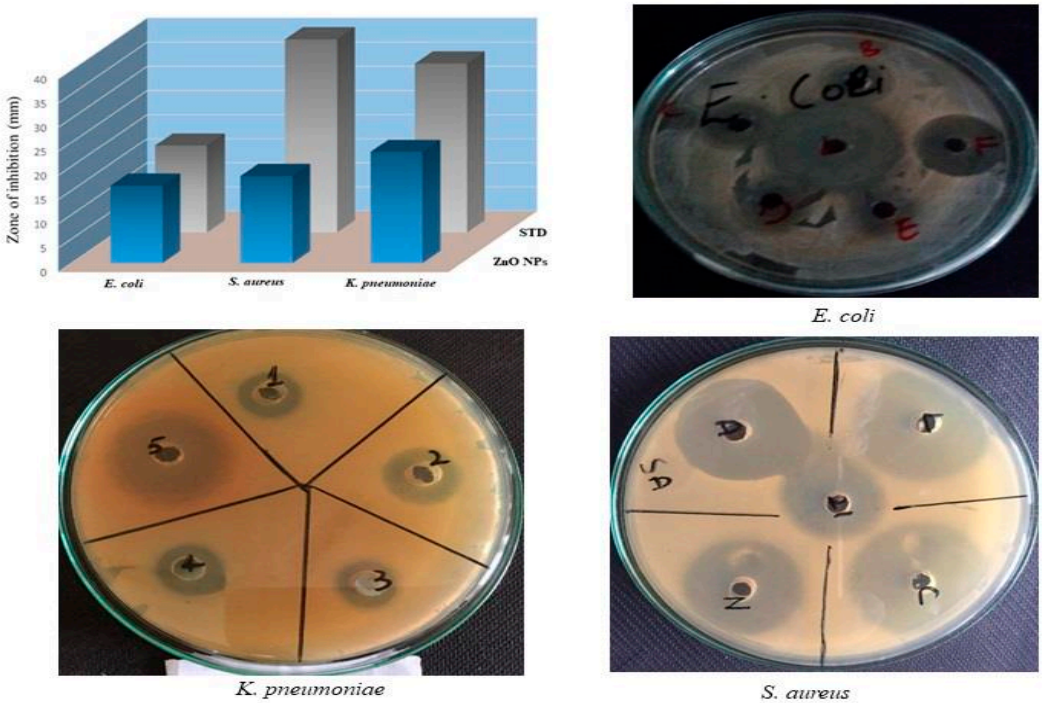

Figure 3. Antibacterial activity of synthesized ZnO NPs against *K. pneumoniae*, *S. aureus* and *E. coli*.

Table 1. Minimum inhibitory concentration (MIC) and minimum bactericidal concentration (MBC) values of biosynthesized ZnO NPs pathogenic bacteria.

S.No	Sample	MIC (µg/mL)			MBC (µg/mL)		
		E. coli	*S. aureus*	*K. pneumoniae*	*E. coli*	*S. aureus*	*K. pneumoniae*
1	ZnNPS	94 ± 0.18	47 ± 0.11	34 ± 0.21	185.43 ± 0.16	94.86 ± 0.84	72.71 ± 0.47
2	Levofloxacin	11.72 ± 0.82	0.35 ± 0.11	50.17 ± 0.41	23.43 ± 1.03	7.82 ± 0.45	97.75 ± 0.9

δ Values are expressed as mean ± SD.

2.5. Membrane Damage Bioassay

The structural strength of the bacterial cell was determined by confirming the cell membrane injury by the biosynthesized ZnO NPs. The results in Figure 4 depict that the treatment of *E. coli*, *S. aureus*, and *K. pneumoniae* with ZnO NPs demonstrated a considerable increase in the concentration of intracellular contents. Moreover, the results clearly showed that the biosynthesized ZnO NPs considerably damaged the test bacterial membrane. Moreover, it has been observed that the membrane-damaging potential of ZnO NPs was increased with the increase in concentration and time of exposure as depicted by the elevated A_{260} values. In the case of *K. pneumoniae*, the membrane was seriously damaged with an A_{260} value of 0.34 at 4 MIC at 120 min of exposure. However, in the case of *S. aureus* and *E. coli*, the A_{260} values for extracellular substances released were 0.31 and 0.28 at 120 min of exposure at 4 MIC, respectively (Figure 4). The basic mechanism behind damaging the bacterial cell might be due to the establishment of hydrogen bonds between the free NH group present in the biosynthesized ZnO NPs and the peptidoglycan layer of the bacterial cell [23].

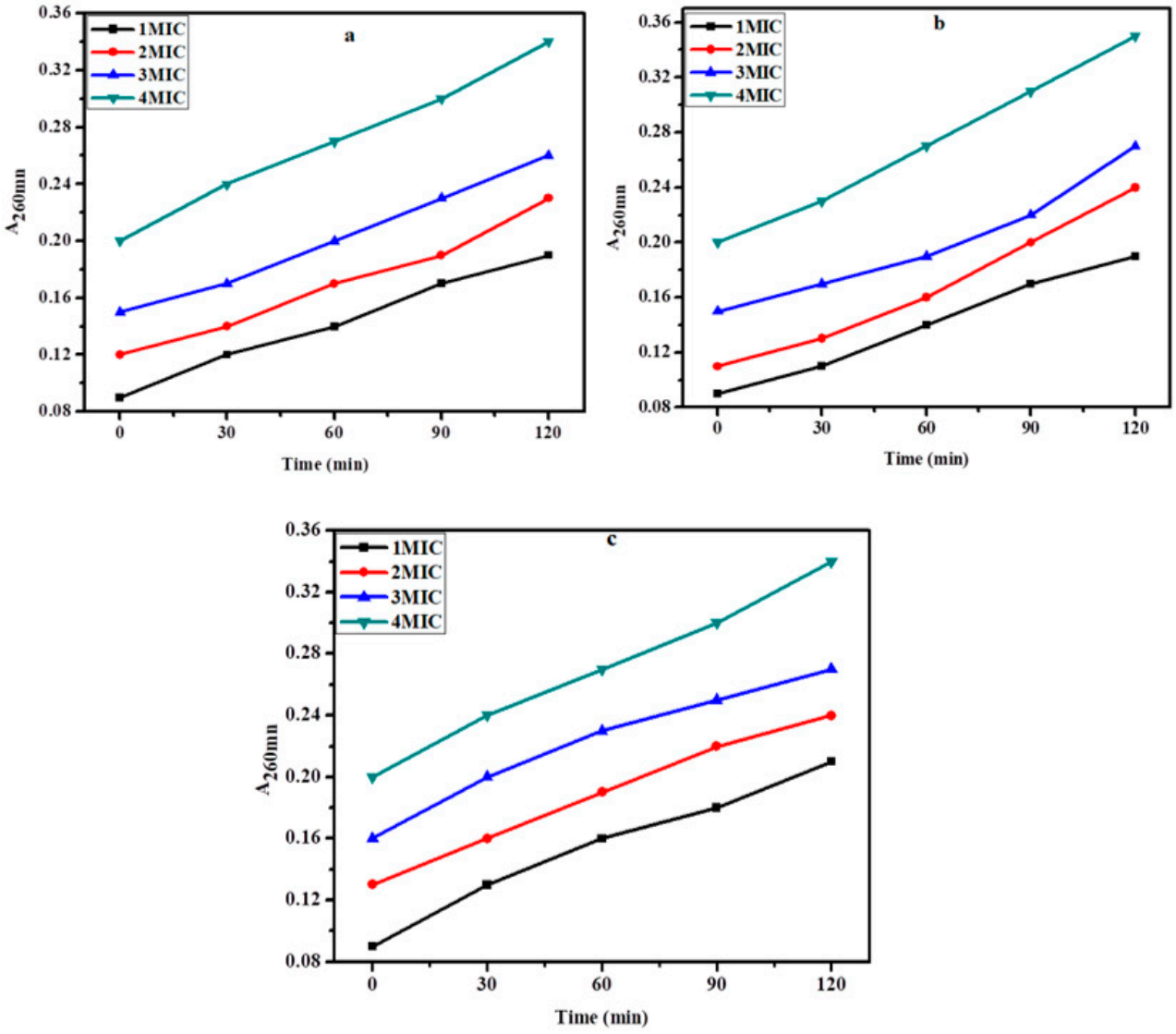

Figure 4. Effect of synthesized ZnO NPs on the release of intracellular materials from (**a**) *E. coli* (**b**) *S. aureus* and (**c**) *K. pneumoniae* cell suspensions at different times and concentrations.

2.6. Inner Membrane Permeability Bioassay

The degradation of the bacterial inner membrane is based on the enzyme β-galactosidase, which is released when bacterial inner membranes are damaged. Lactose serves as β-galactosidase's real substrate and converts ONPG into o-nitrophenol which is a colored product with a wavelength of 420 nm. In the current investigation, the cell suspension was treated with different concentrations, i.e., 1 × MIC, 2 × MIC, 3 × MIC, and 4 × MIC of ZnO NPs, and the cleavage of ONPG was measured for 120 min and the results are plotted in Figure 5a, Figure 5b, and Figure 5c for *E. coli*, *S. aureus* and *K. pneumoniae*, respectively. It has been observed that the hydrolysis rate of ONPG was increased with an increase in the time of interaction of ZnO NPs with the tested bacterial strains. The findings revealed that for all the tested bacterial strains, the utmost hydrolysis rate was recorded at the contact time of 120 min. Moreover, results also showed that the synthesized ZnO NPs exhibited an effective inner membrane damaging potential upon increasing the dose as well as the time of interaction, where a higher A_{420} value suggests high permeability of the bacterial membrane. The potential mechanism for the bactericidal activity of the biosynthesized ZnO NPs could be the membrane binding potential or its passive diffusion via the cell membrane, resulting in the membrane's permeability as shown in Figure 5a–c.

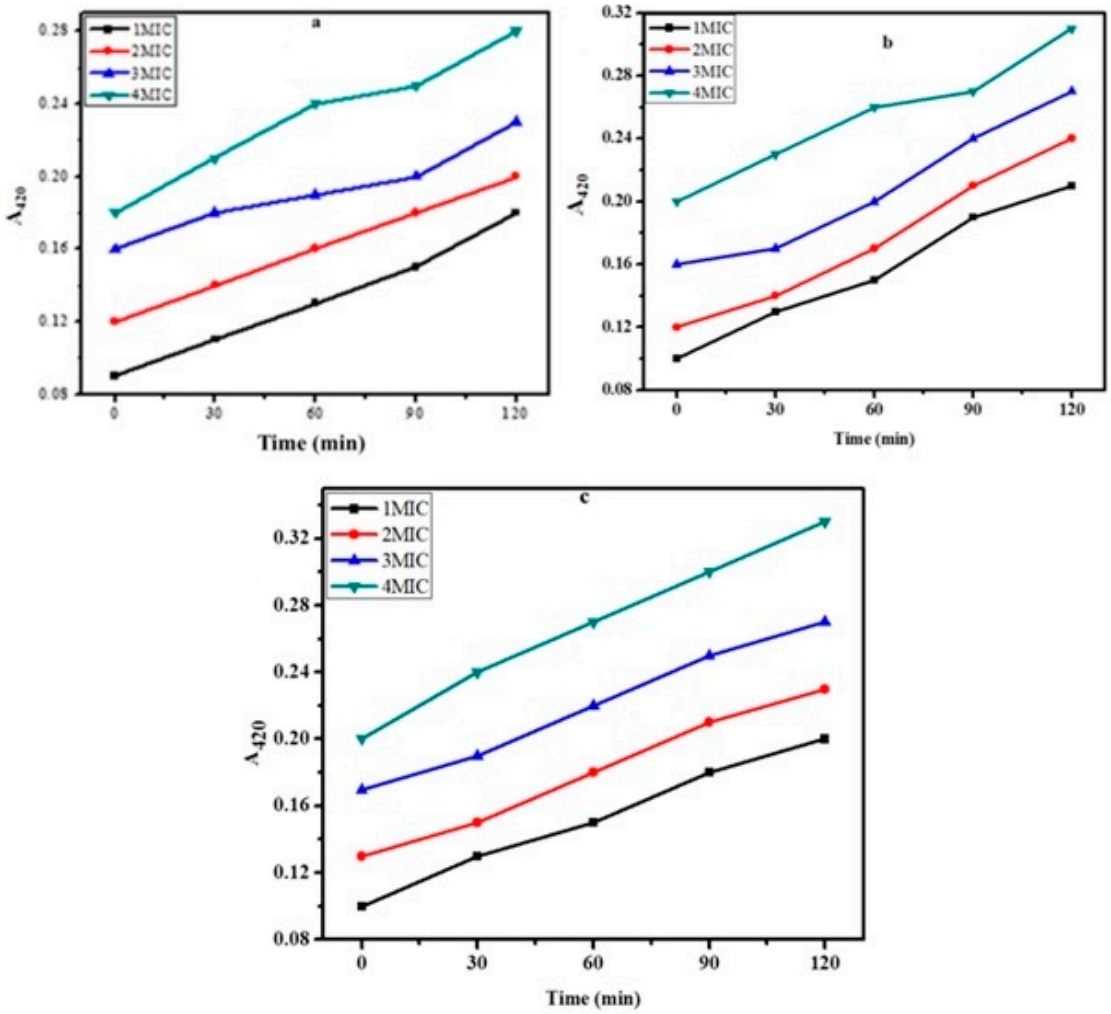

Figure 5. Release of cytoplasmic β-galactosidase from cell suspension of (**a**) *E. coli* (**b**) *S. aureus* (**c**) *K. pneumoniae* treated with synthesized ZnO NPs at different concentrations and times.

2.7. Hemolytic Activity

The results in Figure 6 depict the hemolytic effect of biosynthesized ZnO NPs. The effect was studied at concentrations of 50, 100, 200, and 400 µg/mL of the test sample. The results demonstrated that the test sample caused 1, 1.3, 1.7, and 2.3% lysis of red blood cells at 50, 100, 200, and 400 µg/mL, respectively. Conversely, Triton X-100, a standard hemolytic agent, caused 87% of hemolysis at 400 µg/mL. The comparison revealed that the biosynthesized ZnO NPs showed no hemolysis at 400 µg/mL.

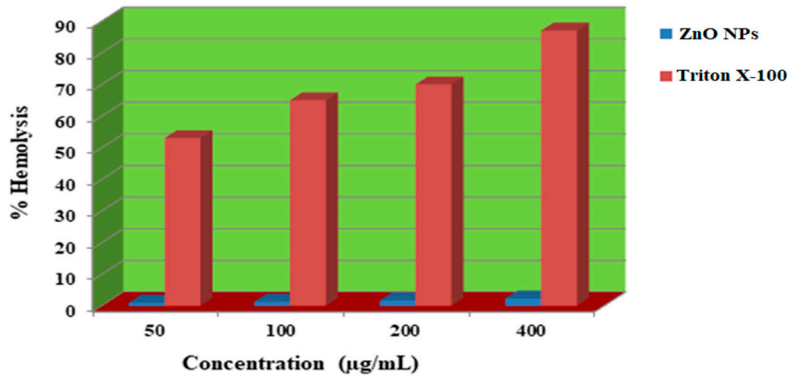

Figure 6. Hemolysis of red blood cells induced by synthesized ZnO NPs.

2.8. Photocatalytic Degradation of Synthetic Methyl Orange Dye

The biosynthesized ZnO NPs were also assessed for the catalytic degradation of the methyl orange dye and the results are presented in Figure 7. It has been observed that without nanoparticles, no dye degradation was recorded, hence confirming that solar irradiation had no effect on dye degradation. The results of the biosynthesized ZnO NPs towards the degradation of methyl orange dye showed a broad absorption peak at 485 nm; however, a continuous decrease in the absorption intensity was recorded with time, hence confirming that the tested ZnO NPs pose a higher ability to degrade the tested dye (Figure 7). The photodegradation of methyl orange dye increased with the increase in contact time. The percent degradation showed that biosynthesized ZnO NPs degrade around 19% dye in 2 h, which increased to 37% and 65% by increasing the irradiation period to 4 h and 6 h, respectively, as shown in Figure 7a,b.

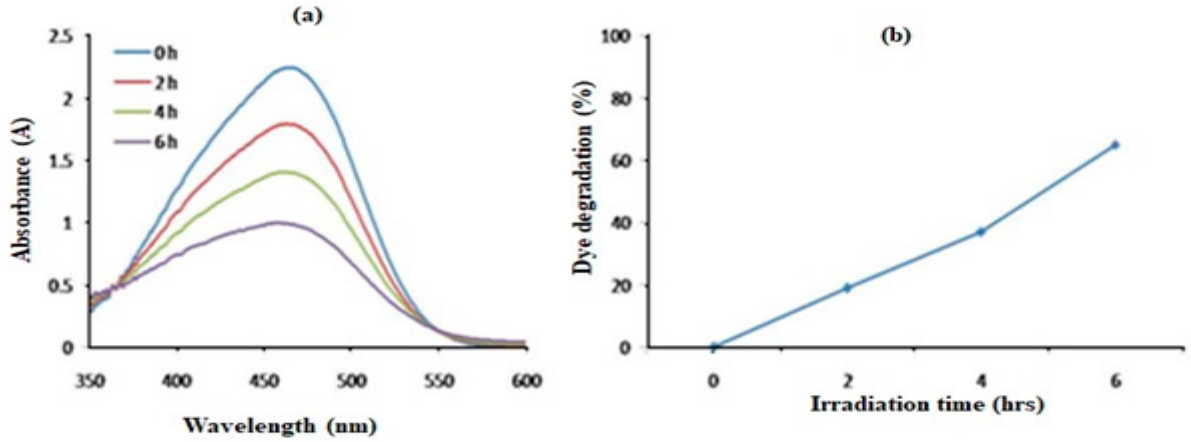

Figure 7. (**a**) Ultraviolet–visible spectrum of methyl orange dye by synthesized ZnO NPs and (**b**) Percent degradation of methyl orange dye by synthesized ZnO NPs.

3. Discussion

The current study made an effort toward the biological fabrication of metal-based nanoparticles using plant parts to synthesize a novel, simple, and non-toxic product that can be utilized for antimicrobial and environmental applications. It is well understood that plants and their parts are considered rich sources of natural products, hence attracting the attention of the scientific community for their wide range of applications including green synthesis of metal nanoparticles [24]. This investigation demonstrates the novel biological synthesis of ZnO NPs from the bark extract of *R. arboreum*, which was tested as an antibacterial agent against clinically isolated pathogenic bacteria and environmental remediation for the photocatalytic degradation of methyl orange dye. *R. arboreum* possesses a wide range of medicinal and antimicrobial applications due to the rich source of phytochemicals such as alkaloids, terpenoids, flavonoids, steroids, saponins, glycosides, tannins, anthraquinones, phlorotannins and reducing sugars [25]. Hence, utilizing *R. arboreum*, these phytochemicals served as both reducing and capping agents for the formation of ZnO NPs. The synthesized ZnO NPs represent characteristic signals in specific wavelength regions in UV–visible spectroscopy as a result of surface plasmon resonance phenomena. However, further characterization analysis revealed its spherical and porous nature with crystalline structure. The characterizations affirm the successful synthesis of ZnO NPs through the active constituents present in the *R. arboreum* bark extract that played an active role in inhibiting the degradation and deformation of the synthesized ZnO NPs. The MIC and MBC values of biosynthesized ZnO NPs were found significant against *E. coli*, *S. aureus*, and *K. pneumoniae*. However, various techniques were used to identify the mechanism of action of eradicating different strains of bacteria through ZnO NPs. The fluorescence microscopy examination was performed to identify the interference of ZnO NPs on the membrane and the cell division apparatus of *B. subtilis* expressing FtsZ-GFP. The results

showed that 70% of the cells exhibited damage in the cytoplasmic membrane after exposure to the ZnO NPs. Electrostatic forces, production of Zn^{2+} ions and the generation of reactive oxygen species were described as possible pathways of the bactericidal action of ZnO NPs. Therefore, understanding the mechanism of ZnO NPs can potentially help in formulating predictive models to fight bacterial resistance [26]. The bacterial cell membrane is a selectively permeable barrier and is considered one of the most important targets for antimicrobial agents [27]. Targeting and degrading this barrier by certain agents leads to negative effects on the bacterial cell, which may ultimately lead to the death of the bacterium cell [28]. It has been observed that biosynthesized ZnO NPs effectively degrade the cell membrane by gradual leakage of compounds with absorbance at 260 nm after treatment with ZnO NPs. Moreover, different types of methods could be utilized for determining the permeability of outer and inner membranes [29]. Determination of the A_{260} value of intracellular compounds is one of the most important techniques for assessing the integrity of the bacterial outer membrane. In the current investigation, it has been observed that the synthesized ZnO NPs possess greater potential to damage the bacterial outer membrane as evidenced by the high A_{260} value. It can be assumed that the green synthesized ZnO NPs had disrupted the lipid–protein interactions in the bacterial membrane which, in turn, caused changes in the membrane permeability, allowing the biosynthesized ZnO NPs to enter into the cell. The ONPG method is widely used for the assessment of the permeability of the inner membrane of bacteria [30]. However, the present finding is based on the fact that the bacteria lose control of the inner membrane permeability as ZnO NPs penetrate the bacterial cell. Moreover, the increased permeability of the bacterial inner membrane was also evident from the elevated production of o-nitrophenol, a colored product resulting from the hydrolysis of ONPG by β-galactosidase. Based on the obtained results, the increase in the permeability of the inner and outer membranes of selected bacterial strains after treatment with ZnO NPs suggested that these two processes may work in concert, which leads to the death of the bacterial cells. Metal nanoparticles have several targets in the bacterial cell but primarily their antibacterial effect is exerted by interacting and damaging bacterial cell membranes [31].

ZnO NPs have good photocatalytic activities towards different dyes; however, the activity could be enhanced through several modification techniques including ZnO nanorods for enhanced phenol degradation [32] and methylene blue toxic dye [33]. In addition, ZnO NPs activity was enhanced with graphene oxide and silver (GO–ZnO–Ag) as nanocomposite for the efficient photodegradation of organic dyes in industrial wastewater [34]. In the current investigation, the synthesized ZnO NPs showed 65% photocatalytic degradation of methyl orange dye at the irradiation period of 6 h. The efficient catalytic activity towards dye degradation is attributed to the unique physiochemical characteristics of the novel nanoparticles synthesized from Zn and *R. arboreum*. Furthermore, the other possible mechanism for effective dye degradation by biosynthesized ZnO NPs is the adsorption of dye over the surface of the nanocomposite in the aqueous media [8]. Following the adsorption, the dyes become excited during sunlight irradiation and the excited dyes transfer e^- into the conduction band of Zn, thus causing the formation of e^- hole pairs (e^-/h^+) [35]. The pairs generate free radicals that are involved in the degradation of methyl orange and yield products such as CO_2 and H_2O [36] The findings of the current investigation confirmed the biosynthesized ZnO NPs as a promising and effective precursor for the remediation of wastewater polluted with organic dye.

4. Materials and Methods

Bacterial strains such as *Escherichia coli* (ATCC 25922), *Staphylococcus aureus* (ATCC 25923) and *Klebsiella pneumoniae* (ATCC 43816) were collected from Pathology Department, Medical Teaching Institute, Hayatabad Medical Complex Peshawar Pakistan as freeze-dried culture and were stored at 4 °C. Growth media such as nutrient agar and nutrient broth and other required solvents used were purchased from Sigma Aldrich, St. Louis, MO, USA.

4.1. Collection of Plant and Preparation of Plant Extract

R. arboreum plant was collected from Seran Valley Khyber Pakhtunkhwa, Pakistan and was authenticated by a botanist at Bacha Khan University, Charsadda-Pakistan. The bark of the collected plant was removed and washed with distilled water to remove the impurities and kept for drying. The dried bark (2.5 kg) was repeatedly extracted with methanol (3 × 5 L) at 25 °C. The methanolic extract was then filtered and further concentrated through a rotary evaporator until brownish crude methanolic extract (~325 g). The crude extract (5 g) was re-suspended in 500 mL of deionized water and was used for the synthesis of ZnO NPs.

4.2. Biosynthesis and Characterization of ZnO NPs

0.01 M zinc chloride ($ZnCl_2$) was mixed with 25 mL of *R. arboreum* extract and stirred for 2 h. The progression of the reaction was monitored through a UV spectrophotometer. The biosynthesized ZnO NPs were then separated from the reaction solution through centrifugation at 6000 rpm for 15 min. The precipitated ZnO NPs were washed thrice with deionized water to remove the impurities and were dried subsequently. Finally, the purified ZnO NPs were subjected to detailed characterization including UV-vis, FTIR, EDX, SEM and XRD as per the standard protocols as shown in Figure 8.

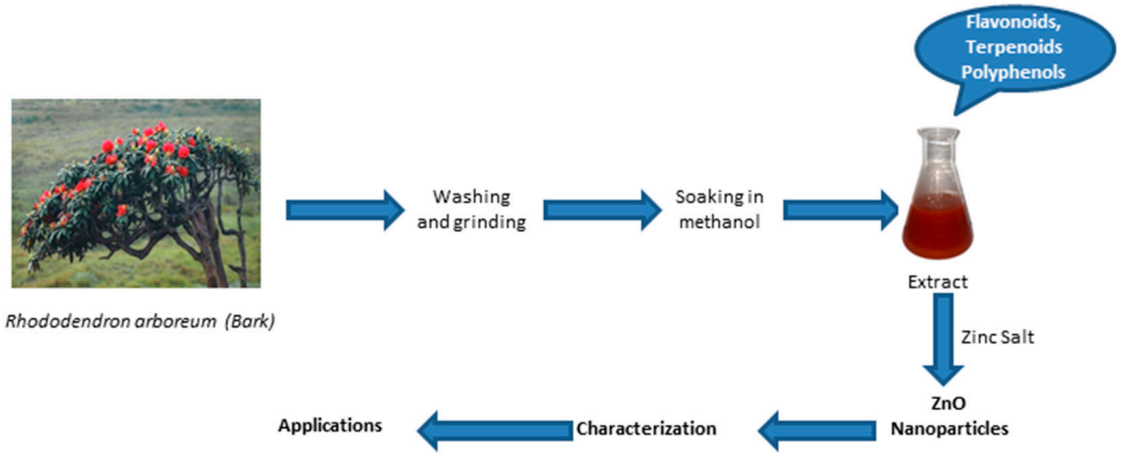

Figure 8. Scheme for green production of ZnO NPs using bark extract of Rhodoendron arboreum.

4.3. Antibacterial Screening

The antibacterial effects of biosynthesized ZnO NPs were assessed using the well diffusion method. The bacterial inoculums comprised of *E. coli*, *S. aureus*, and *K. pneumoniae* were prepared under the instructions made by the National Committee for Clinical Laboratory Standards (NCCLS). Each bacterium was cultured in broth medium and incubated in a shaker incubator at 37 °C for 3 to 4 h until a turbidity of 0.5 McFarland units was attained. With the use of a sterilized cotton swab, the culture of the test bacterium was distributed on the surface of agar plates and left to dry for 3 to 5 min. A sterile cork borer was used to gently bore the wells in the agar plate. The test sample and reference antibiotic were then added to the appropriate well and incubated for 24 h at 37 °C. Using a slightly modified broth dilution method, the minimum inhibitory concentration (MIC) of ZnO NPs was determined. The bacterial culture was injected into tubes with having sterilised broth medium. The test sample was added to the first tube so that the final concentration became 400 µg/mL and was serially diluted in a series of tubes having sterilized broth media to 12.5 µg/mL as the final concentration. The tubes were then incubated for 24 h at 37 °C. MIC was calculated as the lowest concentration of the test sample that inhibited the growth of bacteria. Minimum bactericidal concentration (MBC) of the test sample was obtained by streaking from the tubes used for MIC on agar plates with subsequent incubation for a period of 24 h at 37 °C. The MBC was determined to be the lowest concentration of the test

sample at which the bacterium did not show growth on an agar plate. Results of the test and standard antibiotic levofloxacin were measured in mm.

4.4. Membrane Damage Assay

The effect in terms of cell membrane disturbance was analyzed by measuring the A_{260} value of the intracellular substances that were released upon the interactions of ZnO NPs with the bacterial cells. The culture was refreshed for 24 h by transferring inoculum to broth medium from the agar plate followed by incubation at 37 °C. Centrifugation of the refreshed culture was performed at 10,000 rpm for 10 min. The bacterial pellet collected was thoroughly washed with phosphate-buffered saline (PBS) and suspended again in 0.01 mol L^{-1} PBS solution and the optical density was set to 0.7 at 420 nm. Finally, 1.5 mL of different concentrations of test complexes was treated with 1.5 mL of test bacteria and the quantity of released intracellular substances was measured spectrophotometrically at 260 nm.

4.5. Inner Membrane Permeabilization Bioassay

In this assay, the released β-galactosidase enzyme was determined using the procedure [37]. Test inoculum was prepared in broth medium having 2% of lactose. Then, the bacterial cells were harvested by centrifugation and re-suspended in 0.01 mol L^{-1} PBS solution and the absorbance of the cell suspension was adjusted to 1.2 at 420 nm. Furthermore, test samples (1.6 mL) at different concentrations were added to the culture (1.6 mL) followed by the addition of 150 µL of 30 mM O-nitrophenyl-beta-D-galactopyranoside (ONPG) and thorough mixing of *o*-nitrophenol produced at different time intervals was measured at 420 nm.

4.6. Hemolytic Assay

To avoid blood coagulation, blood samples were taken from human donors in K_2-EDTA tubes. Centrifugation was conducted at 14,000 rpm for 5 min and the plasma was gently aspirated and the cell pellet was washed 3 times with PBS (pH 7.4). Diluted RBCs were mixed with varying concentrations of the test sample (1:1 ratio). Triton X-100 (20%) and PBS were used as positive and negative controls, respectively [38]. All the tubes were shaken for 1 h at 37 °C before being centrifuged for 5 min at 14,000 rpm to pellet the cells. The upper portion was collected in a clean test tube and the absorbance was checked at 540 nm. The following Equation (1) was used for the determination of percent hemolysis.

$$\% \, Hemolysis = \frac{At - An}{Ap - An} \times 100 \quad (1)$$

where

At is the absorbance of the test sample.
An is the absorbance of the negative control (PBS).
Ap is the absorbance of the positive control (Triton-X-100).

4.7. Photocatalytic Degradation of Synthetic Methyl Orange Dye

The synthesized ZnO NPs were also assessed for the degradation of synthetic methyl orange dye using sunlight as a source of energy. Initially, the dye was kept in the sunlight without nanoparticles to ensure zero degradation of dye from solar irradiation. A beaker containing 10 mL methyl orange (25 ppm) and 0.1 mg of nanoparticles was kept in the sunlight with continuous stirring. The photodegradation reactions were conducted at Bacha Khan University, Pakistan, in direct sunshine at coordinates of 39°9° N and 71°44° E. The reaction was first run in complete darkness for 30 min to confirm adsorption and desorption equilibrium. Correspondingly, in direct sunlight, the reactions were performed for 30 min and aliquots of the reaction were taken at predetermined intervals while being exposed to solar light irradiations. At the end of each experimental run, the solution was

centrifuged at 14,000 rpm and was subjected to UV-vis spectrophotometric analysis. For the determination of percent degradation, Equations (2) and (3) were used.

$$\text{Degradation rate } (\%) = \left(\frac{C_o - C}{C_o}\right) \times 100 \quad (2)$$

$$\text{Degradation rate } (\%) = \left(\frac{A_o - A}{A_o}\right) \times 100 \quad (3)$$

where *C*o is the initial dye concentration, *C* is the dye concentration after UV irradiation, *A*o shows initial absorbance, and *A* is the dye absorbance after UV irradiation.

4.8. Statistical Analysis

All the experimental trials were performed in triplicates and data were expressed as mean ± SD. Moreover, one-way analysis of variance (ANOVA) with Tukey's posthoc test was performed to find significant differences ($p < 0.05$).

5. Conclusions

The current study employed a novel green synthesis of ZnO NPs using the bark extract of *R. arboreum*. The biosynthesized ZnO NPs were confirmed by the detailed characterizations including UV-Vis, FTIR, EDX, XRD, and SEM. The biosynthesized ZnO NPs were proved to be a good antibacterial agent inhibiting the growth of *E. coli*, *S. aureus*, and *K. pneumoniae*. Moreover, the MIC and MBC values of the biosynthesized ZnO NPs against *K. pneumoniae*, *S. aureus*, and *E. coli* were 34 ± 0.21 and 11.71 ± 0.47, 47 ± 0.11 and 23.86 ± 0.84 and 94 ± 0.18 and 40.43 ± 0.16 µg/mL, respectively. The biosynthesized ZnO NPs also pose serious damage to the outer and inner membrane in the first phase of exposure causing the death of bacterial cells. However, the utmost membrane damage was observed at 120 min of exposure. Interestingly, biosynthesized ZnO NPs showed no hemolysis in comparison to Triton X-100 a standard hemolytic agent. In addition to the antibacterial activities, the biosynthesized ZnO NPs also exhibited significant catalytic activity towards the degradation of methyl orange dye. The results demonstrated that the rate of photodegradation of methyl orange was increased exposure time and reached 65% by reaching the irradiation period of 6 h. This study therefore concluded that *R. arboreum*-based ZnO NPs are capable of effectively controlling the pathogenic bacteria and can be applied for water purification through photocatalytic degradation of dye. However, the key constraint of using nanoparticles against microbial activities and dye removal is the complete separation from treated media. In this regard, several attempts have been made for the separation for regeneration and recycles back for reuse. However, the dual approach of removal and regeneration is still at the exploratory stage that requires extensive research for successful exploration. Furthermore, keeping the real environmental systems with high microbial and pollutant heterogeneity and complexity in view, there is a dire need to explore the potential of the biosynthesized ZnO NPs in the real environment.

Author Contributions: Writing—original draft, supervision and formal analysis, S.A.; methodology, investigation and formal analysis, S.; validation, revision and editing and formal analysis, T.A. (Tanveer Asghar); writing—original draft, revision and editing and validation, M.I.J.; revision and editing, Data curation and methodology, M.W.; revision and editing, Data curation and Conceptualization, T.A. (Tahir Ali); validation, investigation, funding acquisition, writing—original draft, R.U.; Data curation, funding acquisition, resources, investigation and revision and editing, A.B. All authors have read and agreed to the published version of the manuscript.

Funding: The research work is supported by researchers supporting project number (RSP2024R346) at King Saud University Riyadh Saudi Arabia.

Data Availability Statement: All the available data incorporated in the MS and can be found with Sajid Ali.

Acknowledgments: The authors wish to thank the Researchers Supporting Project number (RSP2024R346) at King Saud University Riyadh Saudi Arabia for financial support.

Conflicts of Interest: The authors declare no conflicts of interest.

References

1. Ahmad, A.; Khan, M.; Sufyan Javed, M.; Hassan, A.M.; Choi, D.; Hassan, K.; Waqas, M.; Ayub, A.; Alothman, A.A.; Almuhous, N.A. Eco-benign synthesis of α-Fe_2O_3 mediated *Trachyspermum ammi*: A new insight to photocatalytic and bio-medical applications. *J. Photochem. Photobiol. A Chem.* **2024**, *449*, 115423. [CrossRef]
2. Darra, R.; Hammad, M.B.; Alshamsi, F.; Alhammadi, S.; Al-Ali, W.; Aidan, A.; Tawalbeh, M.; Halalsheh, N.; Al-Othman, A. Wastewater treatment processes and microbial community. In *Metagenomics to Bioremediation: Applications, Cutting Edge Tools, and Future Outlook*; Academic Press: Cambridge, MA, USA, 2022; pp. 329–355.
3. Salam, M.A.; Al-Amin, M.Y.; Salam, M.T.; Pawar, J.S.; Akhter, N.; Rabaan, A.A.; Alqumber, M.A.A. Antimicrobial Resistance: A Growing Serious Threat for Global Public Health. *Healthcare* **2023**, *11*, 1946. [CrossRef]
4. Sudarshan, S.; Harikrishnan, S.; RathiBhuvaneswari, G.; Alamelu, V.; Aanand, S.; Rajasekar, A.; Govarthanan, M. Impact of textile dyes on human health and bioremediation of textile industry effluent using microorganisms: Current status and future prospects. *J. Appl. Microbiol.* **2023**, *134*, lxac064. [CrossRef] [PubMed]
5. Islam, T.; Repon, M.R.; Islam, T.; Sarwar, Z.; Rahman, M.M. *Impact of Textile Dyes on Health and Ecosystem: A Review of Structure, Causes, and Potential Solutions*; Springer: Berlin/Heidelberg, Germany, 2023.
6. Jorge, A.M.S.; Athira, K.K.; Alves, M.B.; Gardas, R.L.; Pereira, J.F.B. Textile dyes effluents: A current scenario and the use of aqueous biphasic systems for the recovery of dyes. *J. Water Process. Eng.* **2023**, *55*, 104125. [CrossRef]
7. Hasan, S.; Rauf, A. Role of Nanomaterials for Removal of Biomaterials and Microbes from Wastewater. In *Nanotechnology Horizons in Food Process Engineering*; Academic Press: Cambridge, MA, USA, 2023; pp. 303–342.
8. Madhan, G.; Begam, A.A.; Varsha, L.V.; Ranjithkumar, R.; Bharathi, D. Facile synthesis and characterization of chitosan/zinc oxide nanocomposite for enhanced antibacterial and photocatalytic activity. *Int. J. Biol. Macromol.* **2021**, *190*, 259–269. [CrossRef] [PubMed]
9. Motakef-Kazemi, N.; Yaqoubi, M. Green synthesis and characterization of bismuth oxide nanoparticle using mentha pulegium extract. *Iran. J. Pharm. Res.* **2020**, *19*, 70–79. [PubMed]
10. Fritea, L.; Banica, F.; Costea, T.O.; Moldovan, L.; Dobjanschi, L.; Muresan, M.; Cavalu, S. Metal nanoparticles and carbon-based nanomaterials for improved performances of electrochemical (Bio)sensors with biomedical applications. *Materials* **2021**, *14*, 6319. [CrossRef] [PubMed]
11. Mba, I.E.; Nweze, E.I. Nanoparticles as therapeutic options for treating multidrug-resistant bacteria: Research progress, challenges, and prospects. *World J. Microbiol. Biotechnol.* **2021**, *37*, 108. [CrossRef] [PubMed]
12. Thambirajoo, M.; Maarof, M.; Lokanathan, Y.; Katas, H.; Ghazalli, N.F.; Tabata, Y.; Fauzi, M.B. Potential of nanoparticles integrated with antibacterial properties in preventing biofilm and antibiotic resistance. *Antibiotics* **2021**, *10*, 1338. [CrossRef]
13. Islam, M.; Kumar, S.; Saxena, N.; Nafees, A. Photocatalytic Degradation of Dyes Present in Industrial Effluents: A Review. *ChemistrySelect* **2023**, *8*, e202301048. [CrossRef]
14. Hachem, K.; Ansari, M.J.; Saleh, R.O.; Kzar, H.H.; Al-Gazally, M.E.; Altimari, U.S.; Hussein, S.A.; Mohammed, H.T.; Hammid, A.T.; Kianfar, E. Methods of Chemical Synthesis in the Synthesis of Nanomaterial and Nanoparticles by the Chemical Deposition Method: A Review. *BioNanoScience* **2022**, *12*, 1032–1057. [CrossRef]
15. Qamar, S.U.R.; Ahmad, J.N. Nanoparticles: Mechanism of biosynthesis using plant extracts, bacteria, fungi, and their applications. *J. Mol. Liq.* **2021**, *334*, 116040. [CrossRef]
16. Ezealigo, U.S.; Ezealigo, B.N.; Aisida, S.O.; Ezema, F.I. Iron oxide nanoparticles in biological systems: Antibacterial and toxicology perspective. *JCIS Open* **2021**, *4*, 100027. [CrossRef]
17. El Shafey, A.M. Green synthesis of metal and metal oxide nanoparticles from plant leaf extracts and their applications: A review. *Green Process. Synth.* **2020**, *9*, 304–339. [CrossRef]
18. Sidhu, A.K.; Verma, N.; Kaushal, P. Role of Biogenic Capping Agents in the Synthesis of Metallic Nanoparticles and Evaluation of Their Therapeutic Potential. *Front. Nanotechnol.* **2022**, *3*, 801620. [CrossRef]
19. Mehta, J.; Rolta, R.; Salaria, D.; Ahmed, A.; Chandel, S.R.; Regassa, H.; Alqahtani, N.; Ameen, F.; Amarowicz, R.; Gudeta, K. In vitro and in silico properties of Rhododendron arboreum against pathogenic bacterial isolates. *S. Afr. J. Bot.* **2023**, *161*, 711–719. [CrossRef]
20. Sharma, S.; Chaudhary, S.; Harchanda, A. *Rhododendron arboreum*: A Critical Review on Phytochemicals, Health Benefits and Applications in the Food Processing Industries. *Curr. Nutr. Food Sci.* **2021**, *18*, 287–304. [CrossRef]
21. Naz, F.; Saeed, K. Investigation of photocatalytic behavior of undoped ZnO and Cr-doped ZnO nanoparticles for the degradation of dye. *Inorg. Nano-Metal Chem.* **2021**, *51*, 1–11. [CrossRef]
22. Bala, N.; Saha, S.; Chakraborty, M.; Maiti, M.; Das, S.; Basu, R.; Nandy, P. Green synthesis of zinc oxide nanoparticles using Hibiscus subdariffa leaf extract: Effect of temperature on synthesis, anti-bacterial activity and anti-diabetic activity. *RSC Adv.* **2015**, *5*, 4993–5003. [CrossRef]

23. Ali, S.; Ali, H.; Siddique, M.; Gulab, H.; Haleem, M.A.; Ali, J. Exploring the biosynthesized gold nanoparticles for their antibacterial potential and photocatalytic degradation of the toxic water wastes under solar light illumination. *J. Mol. Struct.* **2020**, *1215*, 128259. [CrossRef]
24. Saleem, S.; Ahmed, B.; Khan, M.S.; Al-Shaeri, M.; Musarrat, J. Inhibition of growth and biofilm formation of clinical bacterial isolates by NiO nanoparticles synthesized from Eucalyptus globulus plants. *Microb. Pathog.* **2017**, *111*, 375–387. [CrossRef] [PubMed]
25. Nisar, M.; Ali, S.; Qaisar, M. Preliminary Phytochemical Screening of Flowers, Leaves, Bark, Stem and Roots of Rhododendron arboreum. *Middle-East J. Sci. Res.* **2011**, *10*, 472–476.
26. Mendes, C.R.; Dilarri, G.; Forsan, C.F.; de Moraes Ruy Sapata, V.; Lopes, P.R.M.; de Moraes, P.B.; Montagnolli, R.N.; Ferreira, H.; Bidoia, E.D. Antibacterial action and target mechanisms of zinc oxide nanoparticles against bacterial pathogens. *Sci. Rep.* **2022**, *12*, 2658. [CrossRef] [PubMed]
27. Varela, M.F.; Stephen, J.; Lekshmi, M.; Ojha, M.; Wenzel, N.; Sanford, L.M.; Hernandez, A.J.; Parvathi, A.; Kumar, S.H. Bacterial resistance to antimicrobial agents. *Antibiotics* **2021**, *10*, 593. [CrossRef] [PubMed]
28. Panchal, P.; Paul, D.R.; Sharma, A.; Choudhary, P.; Meena, P.; Nehra, S.P. Biogenic mediated Ag/ZnO nanocomposites for photocatalytic and antibacterial activities towards disinfection of water. *J. Colloid Interface Sci.* **2020**, *563*, 370–380. [CrossRef] [PubMed]
29. Frallicciardi, J.; Melcr, J.; Siginou, P.; Marrink, S.J.; Poolman, B. Membrane thickness, lipid phase and sterol type are determining factors in the permeability of membranes to small solutes. *Nat. Commun.* **2022**, *13*, 1605. [CrossRef]
30. Bouyahya, A.; Abrini, J.; Dakka, N.; Bakri, Y. Essential oils of Origanum compactum increase membrane permeability, disturb cell membrane integrity, and suppress quorum-sensing phenotype in bacteria. *J. Pharm. Anal.* **2019**, *9*, 301–311. [CrossRef] [PubMed]
31. Ahmed, B.; Hashmi, A.; Khan, M.S.; Musarrat, J. ROS mediated destruction of cell membrane, growth and biofilms of human bacterial pathogens by stable metallic AgNPs functionalized from bell pepper extract and quercetin. *Adv. Powder Technol.* **2018**, *29*, 1601–1616. [CrossRef]
32. Uribe-López, M.C.; Hidalgo-López, M.C.; López-González, R.; Frías-Márquez, D.M.; Núñez-Nogueira, G.; Hernández-Castillo, D.; Alvarez-Lemus, M. Photocatalytic activity of ZnO nanoparticles and the role of the synthesis method on their physical and chemical properties. *J. Photochem. Photobiol. A Chem.* **2021**, *404*, 112866. [CrossRef]
33. Supin, K.K.; Parvathy Namboothiri, P.N.; Vasundhara, M. Enhanced photocatalytic activity in ZnO nanoparticles developed using novel Lepidagathis ananthapuramensis leaf extract. *RSC Adv.* **2023**, *13*, 1497–1515.
34. Al-Rawashdeh, N.A.F.; Allabadi, O.; Aljarrah, M.T. Photocatalytic activity of graphene oxide/zinc oxide nanocomposites with embedded metal nanoparticles for the degradation of organic dyes. *ACS Omega* **2020**, *5*, 28046–28055. [CrossRef] [PubMed]
35. Tran, V.A.; Phung, T.K.; Vo, T.K.; Nguyen, T.T.; Nguyen, T.A.N.; Viet, D.Q.; Hieu, V.Q.; Vo, T.-T.T. Solar-light-driven photocatalytic degradation of methyl orange dye over Co_3O_4-ZnO nanoparticles. *Mater. Lett.* **2021**, *284*, 128902. [CrossRef]
36. Jiang, R.; Zhu, H.Y.; Fu, Y.Q.; Jiang, S.T.; Zong, E.M.; Zhu, J.Q.; Zhu, Y.-Y.; Chen, L.-F. Colloidal CdS sensitized nano-ZnO/chitosan hydrogel with fast and efficient photocatalytic removal of congo red under solar light irradiation. *Int. J. Biol. Macromol.* **2021**, *174*, 52–60. [CrossRef] [PubMed]
37. Liu, H.; Du, Y.; Wang, X.; Sun, L. Chitosan kills bacteria through cell membrane damage. *Int. J. Food Microbiol.* **2004**, *95*, 147–155. [CrossRef]
38. Lee, J.K.; Park, S.C.; Hahm, K.S.; Park, Y. A helix-PXXP-helix peptide with antibacterial activity without cytotoxicity against MDRPA-infected mice. *Biomaterials* **2014**, *35*, 1025–1039. [CrossRef]